Transient Thermal Response of Turbulent Compressible Boundary Layers

Hongwei Li[1]
School of Mechanical Engineering,
Purdue University,
West Lafayette, IN 47907

M. Razi Nalim[2]
Department of Mechanical Engineering,
Indiana University-Purdue University,
Indianapolis, IN 46202
e-mail: mnalim@iupui.edu

Charles L. Merkle
School of Mechanical Engineering,
Purdue University,
West Lafayette, IN 47907

A numerical method is developed with the capability to predict transient thermal boundary layer response under various flow and thermal conditions. The transient thermal boundary layer variation due to a moving compressible turbulent fluid of varying temperature was numerically studied on a two-dimensional semi-infinite flat plate. The compressible Reynolds-averaged boundary layer equations are transformed into incompressible form through the Dorodnitsyn–Howarth transformation and then solved with similarity transformations. Turbulence is modeled using a two-layer eddy viscosity model developed by Cebeci and Smith, and the turbulent Prandtl number formulation originally developed by Kays and Crawford. The governing differential equations are discretized with the Keller-box method. The numerical accuracy is validated through grid-independence studies and comparison with the steady state solution. In turbulent flow as in laminar, the transient heat transfer rates are very different from that obtained from quasi-steady analysis. It is found that the time scale for response of the turbulent boundary layer to far-field temperature changes is 40% less than for laminar flow, and the turbulent local Nusselt number is approximately 4 times that of laminar flow at the final steady state. [DOI: 10.1115/1.4003571]

Keywords: boundary layer, turbulent, wave rotor, transient

1 Introduction

Transient heat transfer is often experienced by thermal systems such as heat exchangers, nuclear reactors, turbomachine blades, combustion engines, and various nonsteady flow devices. The design and operation of such devices require the accurate prediction of the time-varying thermal response and cyclic thermal loading. Previous work on transient convective hear transfer includes dimensional analysis of unsteady turbulent boundary layer equations [1], transient heat transfer in internal combustion engines [2], numerical analysis of heat transfer in intensely pulsating turbulent pipe flow [3], and experimental investigation of heat transfer in pulsating pipe flow at varying frequency and Reynolds numbers [4].

Of particular interest for the present work is the flow of gases of varying temperature, which occurs in regenerative heat exchangers [5], shock tubes [6], and wave rotors [7]. Using confined combustion, a wave rotor combustor can achieve significant pressure gain and potentially reduce gas turbine engine fuel consumption and carbon dioxide emissions by about 20% [8]. Wave rotors utilize compressible gas flows, and their inlet port flow fields are likely turbulent in most applications [9]. Turbulence is also important for on-rotor combustion [10]. Further, as cold and hot gases periodically pass through the wave rotor channels, the temperature differences in the gas flow may be significant relative to the absolute temperatures, indicating significant gas density variation. Therefore, the flow compressibility and turbulence in such devices must be considered to predict the heat transfer rate accurately in magnitude and phase variation during the transient heat transfer process.

The unsteady thermal response due to a moving incompressible *laminar* fluid of varying temperature was previously numerically investigated on a 2D semi-infinite flat plate, demonstrating that both the magnitude and the direction of heat transfer can be significantly different from quasi-steady models commonly used [11]. In this paper, the transient turbulent thermal boundary layer due to a moving compressible fluid of varying temperature is numerically studied on a two-dimensional semi-infinite flat plate. The momentum and energy equations become coupled and must be solved simultaneously. The turbulence is modeled using a two-layer eddy viscosity model developed by Cebeci and Smith [12], and the turbulent Prandtl number formulation originally developed by Kays and Crawford [13]. The governing differential equations are discretized with the Keller-box method. The numerical accuracy is ensured by a grid-independence study and validated by comparison with a steady state solution. It is found that the transient time scale for turbulent flow is 40% less than for laminar flow, and the turbulent local Nusselt number is approximately 4 times that of laminar flow at the final steady states.

2 Governing Equations and Boundary Conditions

Transient heat flux is produced when a step change in the far-field temperature is convected past a 2D semi-infinite flat plate. A schematic of the convected temperature change as a discontinuity approaches the leading edge of a plate is shown in Fig. 1, along with the boundary layer on the plate, including the boundary layer transition from laminar to turbulent.

Pressure variations are neglected in this study and the velocity far from the plate is assumed constant. The far-field fluid-temperature and velocity are initially uniform. At time $t=0$, the incoming far-field flow has a sudden temperature step change while the plate remains at rest at its initial temperature. As this step change in temperature sweeps past the plate, the heat flux to the plate responds in a transient manner.

To apply the similarity transformation, the two-dimensional Reynolds-averaged boundary layer equations are written in non-dimensional form as follows:

- continuity equation

[1]Present address: Department of Civil Engineering, Technical University of Denmark, Denmark.

[2]Corresponding author.

Contributed by the Heat Transfer Division of ASME for publication in the JOURNAL OF HEAT TRANSFER. Manuscript received November 9, 2009; final manuscript received January 25, 2011; published online April 26, 2011. Assoc. Editor: Cholik Chan.

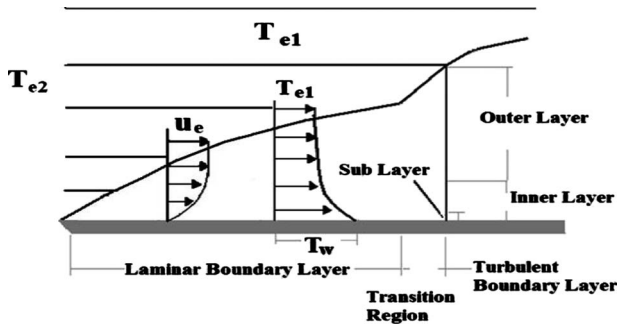

Fig. 1 Convected far-field temperature step change and the boundary layer transition on a 2D semi-infinite flat plate

$$\frac{\partial \hat{\rho}}{\partial \tau} + \frac{\partial \hat{\rho} U}{\partial X} + \frac{\partial \overline{\hat{\rho} V}}{\partial Y} = 0 \tag{1}$$

- x-momentum equation

$$\hat{\rho}\frac{\partial U}{\partial \tau} + \hat{\rho} U \frac{\partial U}{\partial X} + \overline{\hat{\rho} V}\frac{\partial U}{\partial Y} = \frac{\partial}{\partial Y}\left(\hat{\mu}_{\text{eff}}\frac{\partial U}{\partial Y}\right) \tag{2}$$

- energy equation

$$\hat{\rho}\frac{\partial \theta}{\partial \tau} + \hat{\rho} U \frac{\partial \theta}{\partial X} + \overline{\hat{\rho} V}\frac{\partial \theta}{\partial Y} = \frac{\partial}{\partial Y}\left[\left(\frac{\hat{\mu}}{\text{Pr}} + \frac{\hat{\mu}_t}{\text{Pr}_t}\right)\frac{\partial \theta}{\partial Y}\right] + \frac{\gamma - 1}{\gamma}\hat{\mu}_{\text{eff}}\left(\frac{\partial U}{\partial Y}\right)^2 \tag{3}$$

- equation of state

$$\hat{p} = \hat{\rho}\theta \tag{4}$$

The dimensionless variables defined in the governing equations are

$$X = \frac{x}{L}, \quad Y = \frac{y}{L}\sqrt{\text{Re}_L}, \quad U = \frac{u}{u_R}, \quad V = \frac{v}{u_R}\sqrt{\text{Re}_L}$$

$$\tau = \frac{t u_R}{L}, \quad \theta = \frac{T}{T_R}, \quad \hat{\rho} = \frac{\rho}{\rho_R}, \quad \hat{p} = \frac{p}{p_R}, \quad \hat{\mu} = \frac{\mu}{\mu_R} \tag{5}$$

$$\text{Re}_L = \frac{u_R L \rho_R}{\mu_R}, \quad \text{Pr} = \frac{c_p \mu_R}{k}, \quad T_R = \frac{{u_R}^2}{R}$$

The reference velocity u_R is selected as the freestream velocity while the plate length L is used as the reference length. The expression for the reference temperature T_R is derived from a nondimensional analysis of the energy equation. The linear Chapman–Rubesin viscosity law is assumed and the dimensionless kinematic viscosity is expressed as

$$\hat{\mu} = \frac{\mu}{\mu_R} = \frac{T}{T_R} = \theta \tag{6}$$

By combining this expression with the ideal gas relation, the Chapman–Rubesin density-viscosity relation can be derived from Eq. (6)

$$\hat{\rho}\hat{\mu} = \hat{p} \tag{7}$$

In the governing equations, $\overline{\hat{\rho} V}$ is the nondimensionlized term defined as

$$\overline{\hat{\rho} V} = \hat{\rho} V + \overline{\hat{\rho}' V'} \tag{8}$$

The prime marks here denote fluctuations while the bars denote Reynolds-averaged quantities. $\hat{\mu}_{\text{eff}}$ is the nondimensionlized effective turbulent eddy viscosity defined as

$$\hat{\mu}_{\text{eff}} = \hat{\mu} + \hat{\mu}_t \tag{9}$$

where Pr_t is the turbulent Prandtl number defined as the ratio of eddy kinematic viscosity to eddy heat diffusivity, where the eddy kinematic viscosity ν_t and the turbulent eddy heat diffusivity ν_h are defined as

$$\nu_t = \frac{-\overline{u'v'}}{\partial u/\partial y} \tag{10}$$

and

$$\nu_h = \frac{-\overline{T'v'}}{\partial T/\partial y} \tag{11}$$

The governing equations are subject to the following initial and boundary conditions:

- initial condition

$$\begin{gathered} U(X, Y = 0, \ \tau < 0) = 0 \\ V(X, Y = 0, \ \tau < 0) = 0 \\ U(X, Y \to \infty, \ \tau < 0) = U_e \\ \theta(X, Y \to \infty, \ \tau < 0) = \theta_{e1} \end{gathered} \tag{12}$$

- boundary conditions
- at the wall

$$\begin{gathered} U(X, Y = 0, \tau) = 0 \\ V(X, Y = 0, \tau) = 0 \\ \theta(X, Y = 0, \tau) = \theta_w \end{gathered} \tag{13}$$

- at the freestream

$$\begin{gathered} U(X, Y \to \infty) = U_e \\ \theta(X \le \tau, \ Y \to \infty, \ \tau \ge 0) = \theta_{e2} \\ \theta(X > \tau, \ Y \to \infty, \ \tau \ge 0) = \theta_{e1} \end{gathered} \tag{14}$$

where θ_{e1} and θ_{e2} refer to the freestream temperature before and after the step change, respectively.

It is often useful to transform the governing equations with similarity variables to allow generalized solutions. There are several transformations that can simplify the compressible governing equations such as the Dorodnitsyn–Howarth transformation, the von Mises transformation, and the Crocco transformation [14]. The Dorodnitsyn–Howarth transformation is applied in this study. The essence of this transformation is to remove the density from most of the terms in the compressible governing equations and reduce them to incompressible form. The Dorodnitsyn–Howarth transformation was initially derived for laminar compressible flow; however, it has been shown that it is also applicable to turbulent compressible flow [15].

A mass-weighted normal distance is introduced in the transformation, which integrates the density across the boundary layer

$$Y^* = \int_0^Y \frac{\rho}{\rho_R} dY = \int_0^Y \hat{\rho} dY \tag{15}$$

Following the transformation, the governing equations are changed to the following:

- continuity equation

$$\frac{\partial U}{\partial X} + \frac{\partial V^*}{\partial Y^*} = 0 \tag{16}$$

- x-momentum equation

$$\frac{\partial U}{\partial \tau} + U\frac{\partial U}{\partial X} + V^*\frac{\partial U}{\partial Y^*} = \frac{\partial}{\partial Y^*}\left(\hat{\rho}\hat{\mu}_{\text{eff}}\frac{\partial U}{\partial Y^*}\right) \tag{17}$$

- energy equation

$$\frac{\partial \theta}{\partial \tau} + U\frac{\partial \theta}{\partial X} + V^*\frac{\partial \theta}{\partial Y^*} = \frac{\partial}{\partial Y^*}\left[\hat{\rho}\left(\frac{\hat{\mu}}{\text{Pr}} + \frac{\hat{\mu}_t}{\text{Pr}_t}\right)\frac{\partial \theta}{\partial Y^*}\right] + \frac{\gamma - 1}{\gamma}\hat{\rho}\hat{\mu}_{\text{eff}}\left(\frac{\partial U}{\partial Y^*}\right)^2 \tag{18}$$

It is seen that the continuity equation is reduced to a form similar to that in incompressible flow. The stream function concept, which is defined so as to satisfy the two-dimensional incompressible continuity equation, can therefore be introduced as $U = \partial\psi/\partial Y^*$ and $V^* = -\partial\psi/\partial X$.

The similarity transformation provides a great advantage in the solution of laminar flow problems for which the velocity profiles may be approximated as being similar. Similarity transformations are also helpful for solving nonsimilar flows in both the laminar and turbulent regimes. To apply the similarity method, the incompressible Falkner–Skan transformation is introduced in its unsteady form to define the boundary layer similarity variable η and the nondimensional reduced stream function f

$$\eta = Y^*\sqrt{\frac{1}{X}} \tag{19}$$

and

$$\psi = \sqrt{X} f(X, \eta, \tau) \tag{20}$$

Based on the above definitions, the governing equations, Eqs. (16)–(18), are transformed as follows:

- momentum equation

$$(Af'')' + \frac{1}{2}\eta f'' = X\left[f'\frac{\partial f'}{\partial X} - f''\frac{\partial f}{\partial X} + \frac{\partial f'}{\partial \tau}\right] \tag{21}$$

- energy equation

$$(B\theta')' + \frac{\gamma - 1}{\gamma}A(f'')^2 + \frac{1}{2}f\theta' = X\left[f'\frac{\partial \theta}{\partial X} - \theta'\frac{\partial f}{\partial X} + \frac{\partial \theta}{\partial \tau}\right] \tag{22}$$

The number of prime marks on f and θ denotes here the degree of differentiation with respect to η. The parameters A and B are defined to account for compressibility effects

$$A = \hat{\rho}\hat{\mu}(1 + \hat{v}_t^+) = \hat{p}(1 + \hat{v}_t^+)$$

and

$$B = \frac{\hat{\rho}\hat{\mu}}{\text{Pr}}\left(1 + \frac{\hat{v}_t^+\text{Pr}}{\text{Pr}_t}\right) = \frac{\hat{p}}{\text{Pr}}\left(1 + \frac{\hat{v}_t^+\text{Pr}}{\text{Pr}_t}\right) \tag{23}$$

where $\hat{v}_t^+$ is the dimensionless eddy kinematic viscosity, which is defined as

$$\hat{v}_t^+ = \frac{\hat{v}_t}{\hat{v}} \tag{24}$$

The initial conditions are similar to Eq. (12) while the hydrodynamic boundary conditions are transformed from Eqs. (13) and (14) as follows:

- at the wall

$$f(X, 0, \tau) = f'(X, 0, \tau) = 0 \tag{25}$$

- at the freestream

$$f'(X, \infty, \tau) = 1 \tag{26}$$

The thermal boundary conditions are also obtained from Eqs. (13) and (14), however, a dimensionless temperature ratio ϑ is introduced as $\vartheta = (\theta - \theta_{e1})/(\theta_w - \theta_{e1})$ to quantify the temperature step change. With this new variable, the thermal boundary conditions are changed to

$$\vartheta(X \le \tau, \infty, \quad \tau \ge 0) = \frac{\theta_{e2} - \theta_{e1}}{\theta_w - \theta_{e1}} = R_t$$

$$\vartheta(X \ge \tau, \infty, \quad \tau \ge 0) = 0 \tag{27}$$

$$\vartheta(X, 0, \tau) = 1.0$$

3 Turbulence Modeling

The sophistication of a turbulence model should match the complexity of the flow and the required knowledge of the flow field. In the applications considered here, abrupt changes in temperature are considered but not rapid changes in velocity that are likely to generate complex turbulent flows. Freestream turbulence is also not considered; thus, the established models of boundary layer turbulence are deemed appropriate. With application of boundary layer theory, the current work focuses on understanding the time dependent variation of the heat transfer between the flow and the wall in a known constant flow field. A simple algebraic mixing-length turbulence model is considered sufficient for understanding the global characteristics of the transient heat transfer [16]. While there are several eddy viscosity models, the formulation developed by Cebeci and Smith [12] is one of the simplest models with acceptable accuracy in a wide range of flow conditions and for many engineering problems [17]. It has been previously applied to calculate unsteady flow fields [18] and heat transfer problems [19]. In Cebeci's model, the turbulent boundary layer is treated as a composite layer. The inner and outer regions are represented by separate semi-empirical analytical expressions. The interface between these two regions is defined through the continuity of the eddy viscosity.

A number of different turbulent Prandtl number formulations have been proposed. Often, the turbulent Prandtl number is treated as a constant close to unity or as a function of distance y from the wall and of molecular Prandtl number. In this study, a turbulent Prandtl number model originally developed by Kays and Crawford [13] and extended by Weigand et al. [20] is applied.

The fully developed turbulent boundary layer is generally preceded by a laminar boundary layer followed by a transitional region. The on-set of laminar-turbulent transition is determined by the Reynolds number, the turbulent intensity in the freestream, the pressure distribution in the external flow, the roughness of the wall, and the wall heating/cooling conditions [21]. These factors have complex influences on transition. In this study, an abrupt laminar-to-turbulence transition location is specified at a fixed location. The transition Reynolds number is calculated based on the transition location and the freestream flow properties at the initial steady state.

4 Numerical Discretization

The transformed governing equations are solved by the Keller-box numerical discretization method [22,23]. Based on this method, a system of first-order partial differential equations is formed by introducing new dependent variables. All derivatives are approximated by implicit centered-differencing at the center of the η-x grid rectangle. The derived system of nonlinear algebraic equations is then linearized with Newton's method and solved with an efficient block tridiagonal elimination method [17].

The numerical study of the transient thermal boundary layer response due to a step change in the far-field temperature is performed on a 2D semi-infinite flat plate. The working fluid is air with constant molecular Prandtl number (Pr=0.705) and temperature-dependent dynamic viscosity. The boundary layer

momentum and energy equations are coupled by the equation of state expressing the density variation. This coupling makes the momentum equation unsteady even when the freestream velocity is assumed constant.

The sudden change of the freestream temperature introduces a large temperature gradient within the thermal boundary layer. As time progresses, this temperature gradient moves through the boundary layer, starting from the leading edge and moving downstream. At long times, after the flow has passed a given x location, the heat flux approaches the steady heat flux corresponding to the new freestream temperature. To resolve the thermal boundary layer adequately, the grid is stretched in the η direction with $\Delta\eta = 0.0001$ at the wall and a stretch ratio 1.01. In laminar flow, 99% of the freestream velocity is reached at a constant dimensionless boundary layer thickness of approximately $\eta_e = 8.0$. In contrast, the required η_e of a turbulent boundary layer will increase with distance x from the leading edge, in order to keep the far-field boundary layer shear stress $f''_{(\eta=\eta e)}$ less than a specified value at a specific x location [17,19] for adequate accuracy. For convenience, the computational domain is extended to $\eta_e = 41$ in the η direction, which can fully cover the boundary layer thickness variation over the selected plate length.

The velocity and temperature field are solved with uniform grid spacing in the X and τ directions with $\Delta\tau = \Delta X = 0.001$, so that the Courant number is 1.0. The temperature jump in the incoming fluid is treated as a parameter, as noted below. The calculations are performed from the leading edge ($x = 0.0$ m) as laminar flow up to $x = 0.35$ m. The laminar to turbulent transitional occurs at $x = 0.04$ m. Numerical accuracy is verified by computing on finer spatial and temporal grids until no significant solution change was observed.

Applicable experimental work on transient turbulent heat transfer on a flat plate was not found for validation of the transient computational method. Instead, the numerical method and the implementation of turbulent boundary layer models were tested by comparing with other published work for steady turbulent compressible flow and flow friction predictions [19], before extending it to transient problems.

5 Results and Discussion

The convected far-field temperature step change problem is characterized by the dimensionless time ratio $\tau^+ = U_e t/x$. The disturbance generated at the far-field travels with freestream velocity U_e, and reaches a specific x location at $\tau^+ = 1.0$. Upon its arrival, the thermal boundary layer begins the transition from its initial steady state toward the final ultimate steady state under the new thermal boundary conditions. The computational domain in this study is confined in the region upstream of the traveling temperature wave front ($\tau^+ > 1.0$).

Two different cases of thermal boundary conditions are considered in this study: (1) a change in direction of fluid-plate temperature difference and heat transfer (case T-600-300-450) and (2) a decrease in magnitude of fluid-plate temperature difference but with the same direction of heat transfer (case T-500-400-300).

In case T-600-300-450, the freestream temperature is initially at 600 K and, thereafter, step changes to 300 K upon the thermal contact surface arrival. The plate remains at 450 K during the entire thermal transition. Shown in Fig. 2 are the thermal boundary layer temperature profiles for case T-600-300-450 at several instants of times at a given X location ($X = 0.16$, i.e., $x = 0.16$ m with a reference length of 1.0 m). The transition Reynolds number calculated based on the initial freestream temperature is $\mathrm{Re}_{tr} = 2.1 \times 10^5$. The uniform freestream velocity is set to 313 m/s, corresponding to $M = 0.9$ at a far-field temperature at 300 K.

Case T-600-300-450 has a temperature step change ratio $R_T = 2.0$. The temperature difference between the wall and the freestream changes sign during the thermal transition. The thermal response starts at $\tau^+ = 1$. The transient thermal boundary layer approaches its ultimate steady state (which is defined as the state when the transient local Nusselt number reaches 99.9% that of the final steady state) very closely by $\tau^+ = 1.5$. Comparing with previously reported laminar thermal boundary layer transition time scale estimated at $\tau^+ = 2.5$ [11], the turbulent thermal boundary layer transition is much faster. The fast thermal boundary layer transition of turbulent flow is attributed to the much larger turbulent mixing rates compared with the relatively low molecular diffusion rate.

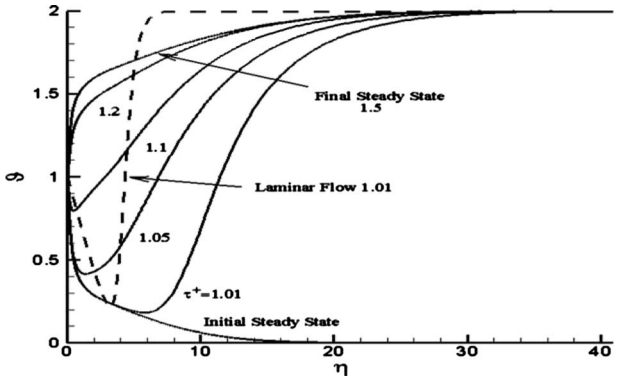

Fig. 2 Transient temperature profiles for case T-600-300-450 with temperature step change ratio $R_T = 2.0$

The thermal response occurs first in the outer boundary layer region, which adjusts to the new far-field boundary condition rapidly. The inner part of the boundary layer remains close to its initial steady state. A temperature extremum is formed between these two regions. Based on its conventional definition, the heat transfer coefficient becomes negative during this transient process.

Comparing with laminar flow (dotted curve at $\tau^+ = 1.01$), the enhanced turbulent mixing rate makes the temperature profile more flat in the region close to the plate. At the steady state, the turbulent temperature profile is convex/concave at $\eta = 2.0$ and the temperature distribution becomes more uniform beyond this point. At the final state, the thermal boundary layer thickness for turbulent flow is approximately 4 times that of the laminar flow in the transformed coordinate.

Affected by the related density variation, the velocity profile also goes through a transition. The corresponding boundary layer velocity profiles during the transition from initial steady state to the final steady state at $\tau^+ = 1.5$ are shown in Fig. 3.

The scaled local Nusselt number after the nondimensionalization and similarity transformation is expressed as

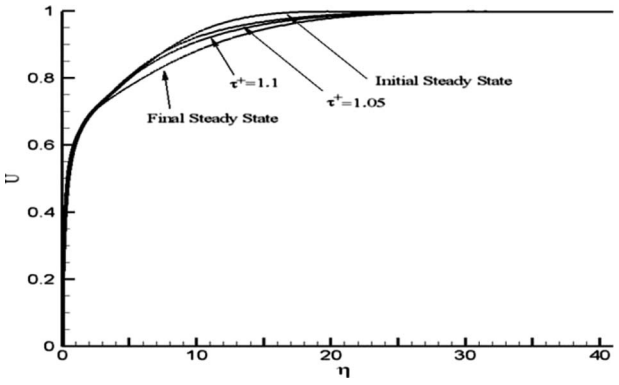

Fig. 3 Transient velocity profiles for case T-600-300-450 with temperature step change ratio $R_T = 2.0$

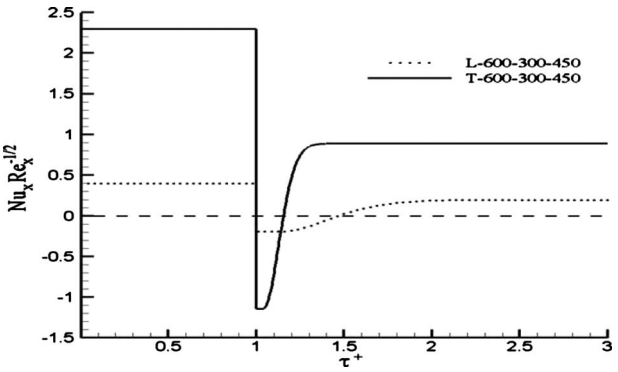

Fig. 4 Scaled nondimensional local Nusselt number transient variation for turbulent flow case T-600-300-450 and laminar flow case L-600-300-450 with temperature step change ratio R_T =2.0

$$\mathrm{Nu}(x,t)\mathrm{Re}_x^{-1/2} = \frac{-\sqrt{\hat{\nu}_e}\hat{\rho}_w}{(\theta_w-\theta_e)}\left.\frac{\partial\theta}{\partial\eta}\right|_{\eta=0} = \frac{-\sqrt{\hat{\nu}_e}\hat{\rho}_w}{1-Rt}\left.\frac{\partial\vartheta}{\partial\eta}\right|_{\eta=0} \tag{28}$$

The scaled nondimensional local Nusselt number variation for case T-600-300-450 is shown in Fig. 4. The laminar flow case L-600-300-450 is plotted for the comparison. For each case, the local Nusselt number becomes negative at the beginning of thermal transition ($\tau^+ \geq 1$) until the temperature extremum disappears (as shown in Fig. 2) in the later transient stages. The local Nusselt numbers for laminar and turbulent flows overlap during the early transient stages. The laminar flow may have a higher heat transfer rate at some time ranges. Upon reaching their final ultimate steady states, the turbulent local Nusselt number is approximately 4 times that of laminar flow.

As shown in Fig. 2, for both flows, initially, the temperature gradient adjacent to the wall remains at its initial steady state while the temperature difference between the wall and the freestream has already changed direction. The local Nusselt number, based conventionally on the boundary layer temperature difference, becomes negative by definition but has little change for the beginning short time period. For laminar flow, this time period ranges from $\tau^+=1.0$ to $\tau^+=1.2$, which indicates that the flow field close to the plate has little temperature change during this period. However, such time period for turbulent flow is much shorter.

The thermal transition time is defined from the initiation of the freestream temperature step change to the final ultimate steady state. The thermal transition times are different between laminar and turbulent flows (Fig. 4). Turbulent flow takes 1.5 ms to complete its thermal transition while laminar flow takes longer time at 2.5 ms.

To better illustrate the transient thermal boundary layer variation, color-shaded contour plots of temperature at different times are plotted in the physical x, y, and t domains in Fig. 5. The temperature contours are plotted at the time that corresponds to the τ^+ values in Fig. 2, i.e., the initial steady state, $\tau^+=1.01$ and $\tau^+=1.2$ at the location $x=0.16$ m. The last plot at $\tau^+=2.5$ represents the time when the new steady states are established in most of the selected computational domain.

The initial steady state is shown in Fig. 5(a). The transition starts at time $t=0$ when the freestream temperature step change convects from the far-field to the leading edge. The contact surface, which separates the two fluids with different temperatures, moves at the freestream velocity. In the freestream, the hot fluid is pushed downstream by the incoming cold fluid. Shown in Fig. 5(b) is the moment immediately after the contact surface passes $x=0.16$ m at time $t=0.52$ ms. Due to viscous effects, some fluid with hot temperature is retained in the region immediately upstream of the contact surface, which temporarily induces a bidirectional heat transfer. Figure 5(c) shows the contact surface con-

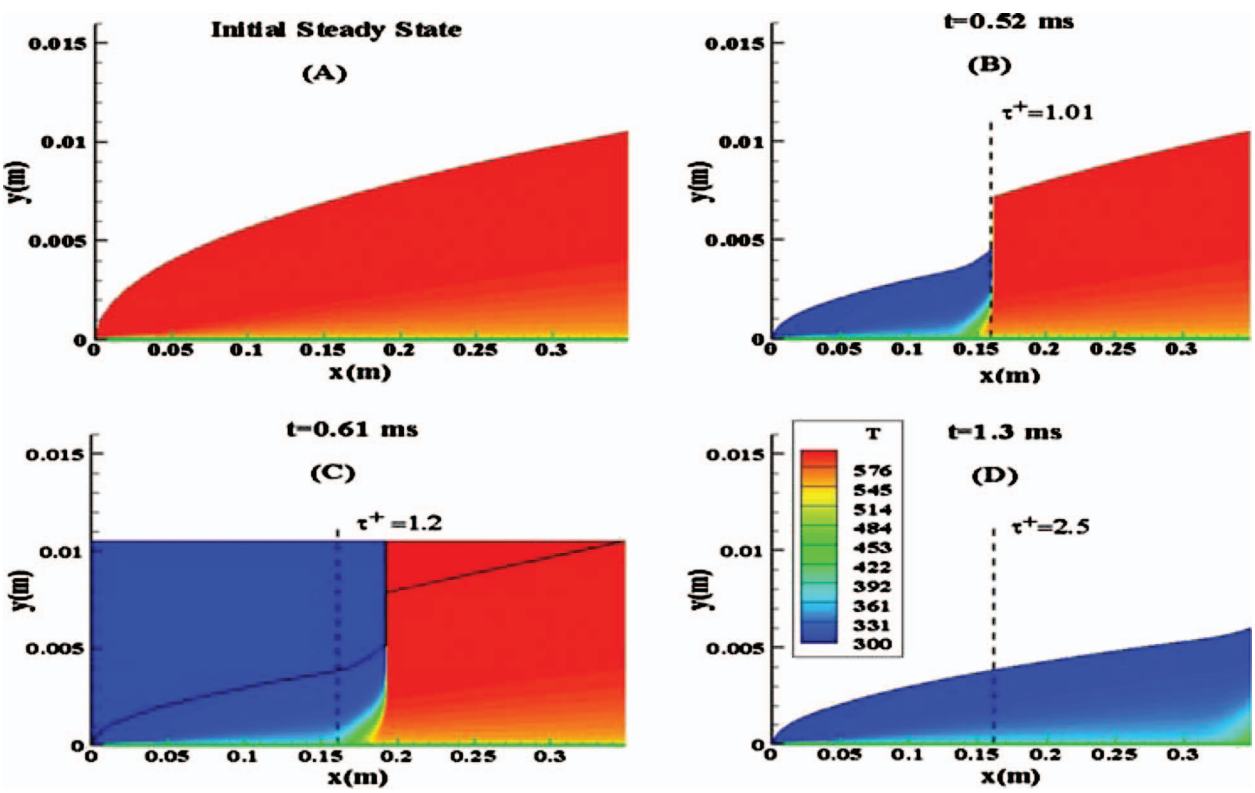

Fig. 5 Temperature contours for case T-600-300-450 with temperature step change ratio R_T=2.0

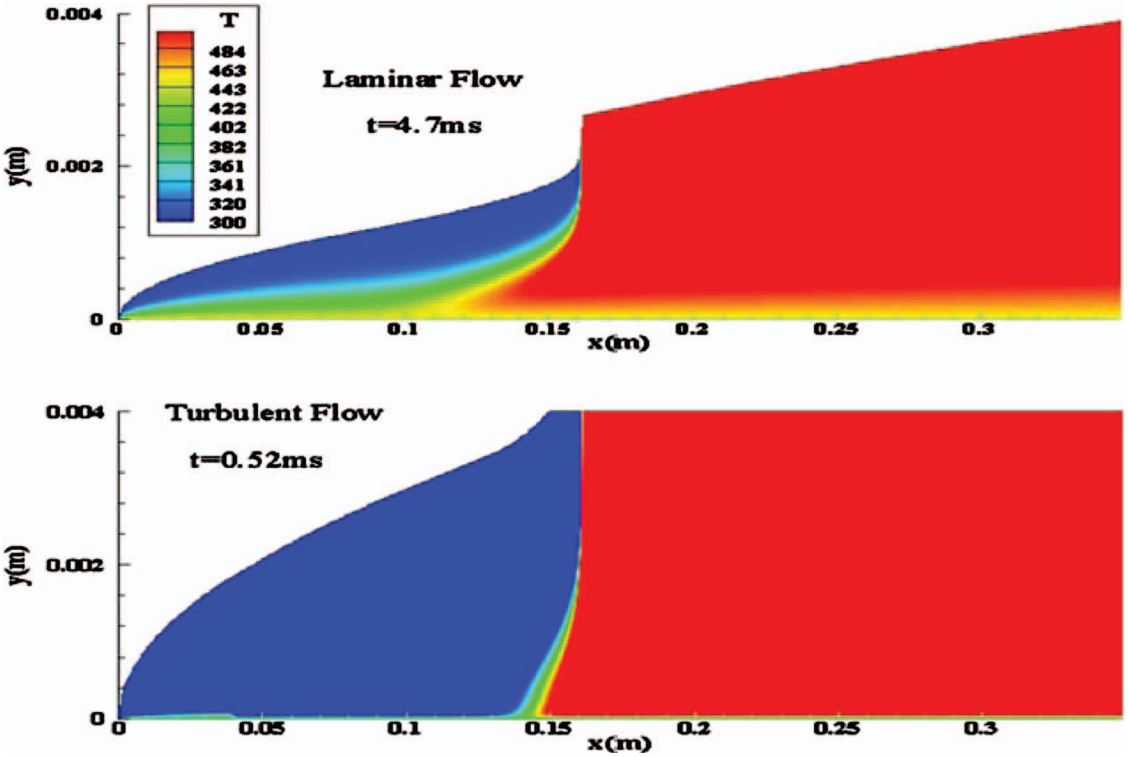

Fig. 6 Temperature contour comparison between cases T-600-300-450 and L-600-300-450

vected further downstream to $x=0.19$ m at $t=0.61$ ms. Figure 5(*d*) shows the moment when the contact surface has been completely swept out of the computational domain.

It may be noted that temperature is shown only in the dimensional computational domain, which is determined by the specification of $\eta_e=41$. The real physical flow domain extends into the freestream, as illustrated in Fig. 5(*c*). The curvilinear shapes of the dimensional computational domain in the temperature contours are determined by the flow thermal properties as well as the longitudinal distance away from the leading edge.

The transient variation of the local Nusselt number is ultimately determined by the temperature variation within the thermal boundary layer; therefore, the differences of local Nusselt number variation between laminar and turbulent flows are also reflected in their temperature contours. The temperature contours when the thermal contact surface arrives at $x=0.16$ m are shown in Fig. 6 for laminar and turbulent flows. The temperature levels are scaled between 300 K and 500 K, in order to make the thermal boundary layer region near the thermal contact surface more distinguishable.

In turbulent flow, the retained hot gas is aggregated in a region close to the contact surface while for laminar flow, this retained hot gas penetrates much further upstream of the contact surface. The unique feature of the retained hot gas distribution for laminar and turbulent flows determines the important transient time scale difference between the two flows. It is clear that the further the penetration of the retained hot gas upstream of the contact surface, the longer the time required to sweep out the previous thermal boundary condition effect and to re-establish the new steady state. This explains why the thermal transition time for laminar flow takes longer than for turbulent flow. On the other hand, as the previous thermal boundary condition has smaller impact for turbulent flow, the response to the freestream temperature step change for turbulent flow is much faster than for laminar flow. It may be noted that the local Nusselt number begins responding relatively early for turbulent flow, whereas it remains constant for a significant time for laminar flow, as illustrated in Fig. 4.

As a comparison, case T-500-400-300 with a temperature step change ratio $R_T=0.5$ is studied to illustrate the thermal response when the heat is monotonically transferred in the initial direction during the thermal transient. In this case, the freestream temperature is initially at 500 K and, thereafter, step changes to 400 K upon arrival of the thermal contact surface. The plate remains at 300 K. The transition Reynolds number calculated based on the initial freestream temperature is $\mathrm{Re}_{tr}=2.9\times10^5$. The transient turbulent temperature profiles at different τ^+ are shown in Fig. 7, together with the comparison of laminar flow at $\tau^+=1.01$. Similar to that described in the $R_T=2.0$ case, the transient temperature profiles at $R_T=0.5$ has a temperature extremum at some η during the thermal transient but becomes monotone again in the final steady state. The extremum disappears as it reaches the wall. At the wall, the direction of heat transfer remains the same but the magnitude changes; the conventional heat transfer coefficient, as defined by the far-field temperature, remains positive.

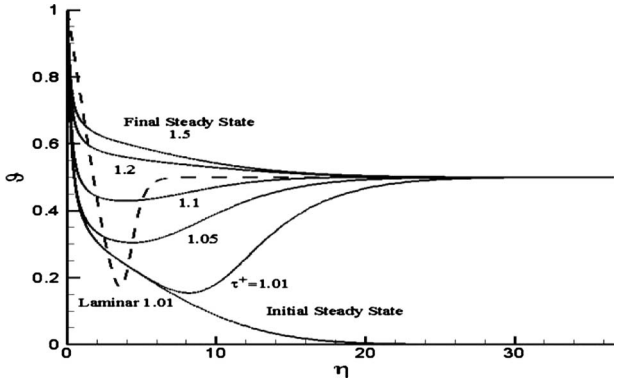

Fig. 7 Transient temperature profiles for case T-500-400-300 with temperature step change ratio $R_T=0.5$

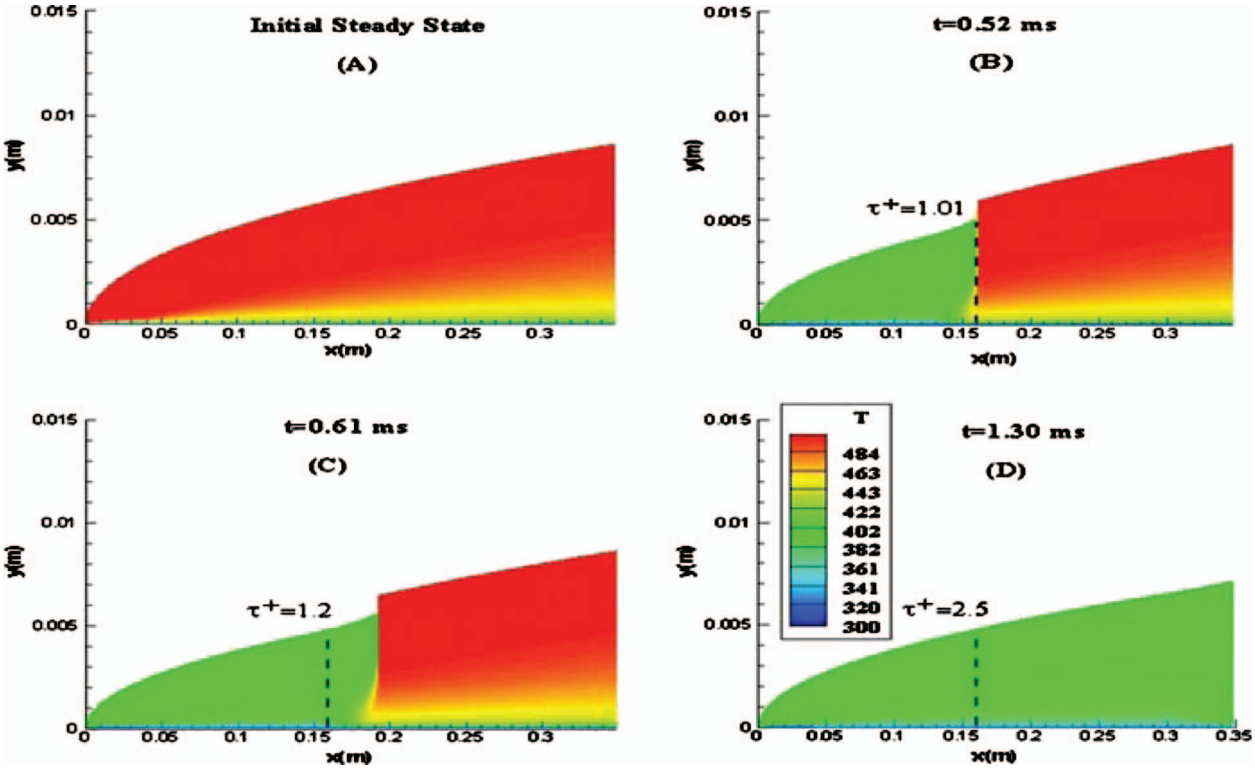

Fig. 8 Temperature contours for case T-500-400-300 with temperature step change ratio R_T=0.5

The transient temperature contours are plotted in Fig. 8. Similar to the previous cases, in the region immediately upstream of the contact surface, the flow with temperature higher than the incoming freestream temperature is retained due to the flow viscosity. This hot fluid hinders the formation of the thermal boundary layer developed under the new boundary conditions.

The scaled nondimensional local Nusselt number variation is shown in Fig. 9 with the comparison for laminar flow. As the fluid-temperature difference does not change sign, the Nusselt number remains positive. The heat transfers monotonically from the fluid to the plate, with only the magnitude of the heat transfer rate varying during the thermal transition. The Nusselt number has a sudden jump at the beginning and then gradually decreases to reach its final steady state value.

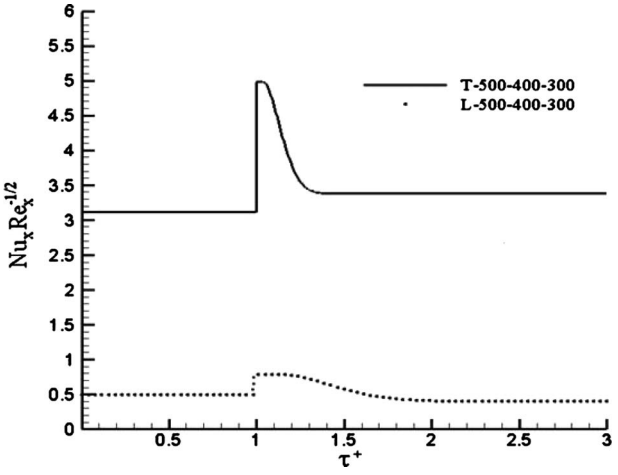

Fig. 9 Scaled nondimensional local Nusselt number transient variation for turbulent flow case T-500-400-300 and laminar flow case L-500-400-300 with temperature step change ratio R_T =0.5

6 Conclusion

The transient thermal response due to a far-field flow temperature step change is numerically studied on a 2D semi-infinite flat plate for turbulent compressible flow. The heat transfer changes both in magnitude and in direction during thermal boundary layer transition, which underscores the need to avoid quasi-steady approximation. Compared with the laminar flow case, the turbulent flow is predicted to have a shorter thermal transition time and a significantly higher heat transfer rate. Nevertheless, the transition time is still significant relative to the cyclic time of gas temperature variation in wave rotors.

The turbulent compressible flow assumption reflects realistic flow conditions of unsteady energy conversion devices. Accurate knowledge of unsteady turbulent heat transfer will enhance the understanding of transient heat transfer characteristics in unsteady flow devices, such as the wave rotor, to improve their design, safety, and transient operation while providing accurate performance evaluation.

Acknowledgment

This work was partially supported by the Rolls-Royce North American Technologies "LibertyWorks," by the Indiana 21st Century Fund for Research and Technology, and by an IUPUI fellowship to HL during this effort.

Nomenclature

A, B = coefficient in the transformed compressible equation
f = nondimensional reduced stream function
h = heat transfer coefficient
k = thermal conductivity

L = characteristic length
Nu = Nusselt number
p = pressure
q = heat transfer rate
Re = Reynolds number
R_T = temperature step change ratio
$\mathrm{Pr}, \mathrm{Pr}_t$ = Prandtl number and turbulent Prandtl number
T = temperature
t = time
u, U = longitude velocity
v, V = transverse velocity
x, X = longitude coordinate
y, Y = transverse coordinate
Y^* = mass-weighted normal distance
η = similarity variable
ρ = density
μ = kinematic viscosity
θ, ϑ = dimensionless temperature
τ = dimensionless time
ψ = stream function
τ^+ = dimensionless time, relative to local contact surface arrival

Subscripts

e = freestream
eff = effective turbulent quantities
t = turbulent
w = wall

References

[1] Zeng, P., 2004, "Unsteady Convective Heat Transfer Modeling and Application to Internal Combustion Engines," Ph.D. thesis, University of Michigan.
[2] Loubar, K., Bellettre, J., and Tazerout, M., 2005, "Unsteady Heat Transfer Enhancement Around an Engine Cylinder in Order to Detect Knock," ASME J. Heat Transfer, **127**(3), pp. 278–286.
[3] Wang, X., and Zhang, N., 2005, "Numerical Analysis of Heat Transfer in Pulsating Turbulent Flow in a Pipe," Int. J. Heat Mass Transfer, **48**, pp. 3957–3970.
[4] Zohir, A. E., Habib, M. A., Attya, A. M., and Eid, A. I., 2006, "An Experimental Investigation of Heat Transfer to Pulsating Pipe Air Flow With Different Amplitudes," Heat Mass Transfer, **42**, pp. 625–635.
[5] Atthey, D. R., 1988, "An Approximate Thermal Analysis for a Regenerative Heat Exchanger," Int. J. Heat Mass Transfer, **31**, pp. 1431–1441.
[6] Fujii, N., Koshi, M., Ando, H., and Asaba, T., 1979, "Evaluation of Boundary-Layer Effects in Shock-Tube Studies of Chemical Kinetics," Int. J. Chem. Kinet., **11**, pp. 285–304.
[7] Nalim, M. R., 2000, "Longitudinally Stratified Combustion in Wave Rotors," J. Propul. Power, **16**, pp. 1060–1068.
[8] Nalim, M. R., Li, H., and Akbari, P., 2009, "Air-Standard Aero-Thermodynamic Analysis of Gas Turbine Engines With Wave Rotor Combustion," ASME J. Eng. Gas Turbines Power, **131**, p. 054506.
[9] Welch, G. E., 1996, "Macroscopic Balance Model for Wave Rotors," AIAA 34th Aerospace Science Meeting and Exhibit, Reno, NV.
[10] Nalim, M. R., 1999, "Assessment of Combustion Modes for Internal Combustion Wave Rotors," ASME J. Eng. Gas Turbines Power, **121**, pp. 265–271; (also Report No. NASA TM 107000, Paper No. AIAA-95-2801, 1995).
[11] Li, H., and Nalim, M. R., 2008, "Thermal Boundary Layer Response to Convected Far-Field Fluid Temperature Changes," ASME J. Heat Transfer, **130**, p. 101001; (also ASME Paper No. IMECE2007-42188, Seattle, 2007).
[12] Cebeci, T., and Smith, A. M. O., 1974, *Analysis of Turbulent Boundary Layers*, Academic, New York.
[13] Kays, W. M., and Crawford, M. E., 1993, *Convective Heat and Mass Transfer*, 3rd ed., McGraw-Hill, New York.
[14] Stewartson, K., 1963, *The Theory of Laminar Boundary Layers in Compressible Fluids*, Oxford University Press, Oxford.
[15] He, J., Kazakia, J. Y., and Walker, J. D. A., 1990, Embedded Function Methods for Supersonic Turbulent Boundary Layers, Paper No. AIAA-90-0306.
[16] Wilcox, D. C., 2006, *Turbulence Modeling for CFD*, 3rd ed., DCW Industries, California.
[17] Cebeci, T., and Bradshaw, P., 1988, *Physical and Computational Aspects of Convective Heat Transfer*, Springer-Verlag, New York.
[18] Cebeci, T., 1977, "Calculation of Unsteady Two-Dimensional Laminar and Turbulent Boundary Layers With Fluctuations in External Velocity," Proc. R. Soc. London, Ser. A, **355**, pp. 225–238.
[19] Kafoussias, N. G., and Xenos, M. A., 2000, "Numerical Investigation of Two-Dimensional Turbulent Boundary-Layer Compressible Flow With Adverse Pressure Gradient and Heat and Mass Transfer," Acta Mech., **141**, pp. 201–223.
[20] Weigand, B., Ferguson, J. R., and Crawford, M. E., 1997, "An Extended Kays and Crawford Turbulent Prandtl Number Model," Int. J. Heat Mass Transfer, **40**, pp. 4191–4196.
[21] Schlichting, H., and Gersten, K., 2001, *Boundary Layer Theory*, 8th ed., Springer-Verlag, Berlin.
[22] Keller, H. B., 1978, "Numerical Methods in Boundary-Layer Theory," Annu. Rev. Fluid Mech., **10**, pp. 417–433.
[23] Cebeci, T., and Jean, C., 2005, *Modeling and Computation of Boundary Layer Flows*, 2nd ed., Springer, New York.